


Enhanced symmetry energy may bear universality of *r*-process abundances

José Nicolás Orce ^{1,2,★}, Balaram Dey,^{3,★} Cebo Ngwetsheni,¹ Srijit Bhattacharya,⁴ Deepak Pandit,^{5,6,★}
Brenden Lesch¹ and Andile Zulu¹

¹*Department of Physics & Astronomy, University of the Western Cape, P/B X17, 7535 Bellville, South Africa*

²*National Institute for Theoretical and Computational Sciences (NITheCS), Stellenbosch, South Africa*

³*Department of Physics, Bankura University, Bankura, 722155 West Bengal, India*

⁴*Department of Physics, Barasat Govt. College, Barasat, 700124 West Bengal, India*

⁵*Variable Energy Cyclotron Centre, 1/AF-Bidhannagar, 700064 Kolkata, India*

⁶*Homi Bhabha National Institute, Training School Complex, Anushaktinagar, 400094 Mumbai, India*

Accepted 2023 August 18. Received 2023 June 20; in original form 2022 May 6

ABSTRACT

The abundances of about half of the elements heavier than iron are subtly attuned by the rapid neutron capture process or *r*-process, which is intimately related to the competition between neutron capture, photo-disintegration, and β -decay rates, and ultimately depends on the binding energy of neutron-rich nuclei. The well-known Bethe–Weizsäcker semi-empirical mass formula describes the binding energy of ground states – i.e. nuclei with temperatures of $T = 0$ MeV – with the symmetry energy parameter converging between 23 and 27 MeV for heavy nuclei. We find an unexpected enhancement of the symmetry energy well above the ground state – at higher temperatures of $T \approx 0.7$ –1.0 MeV – from the available data of giant dipole resonances built on excited states. Although these are likely the temperatures where seed nuclei are created – during the cooling down of the ejecta following neutron-star mergers or collapsars – the fact that the symmetry energy remains constant between $T \approx 0.7$ and 1.0 MeV, may suggest an enhanced symmetry energy at lower temperatures, where neutron-capture may start occurring. Calculations using this relatively larger symmetry energy yield a reduction of the binding energy per nucleon for heavy neutron-rich nuclei and inhibits radiative neutron-capture rates. This results in a substantial close in of the neutron drip line which may elucidate the long sought universality of heavy-element abundances through the *r*-process; as inferred from the similar abundances found in extremely metal-poor stars and the Sun. Sensitivity studies of *r*-process network calculations have been performed using more sophisticated mass models.

Key words: nuclear reactions, nucleosynthesis, abundances – techniques: spectroscopic – Sun: abundances – stars: abundances – transients: neutron star mergers – transients: supernovae.

1 MOTIVATION

The binding energy of a nucleus with Z protons and N neutrons can be described by the well-known Bethe–Weizsäcker semi-empirical mass formula (SEMF) (Weizsäcker 1935; Bethe & Bacher 1936),

$$B(Z, A) = a_v A - a_s A^{2/3} - a_c Z(Z-1)A^{-1/3} - a_{\text{sym}}(A) \frac{(A-2Z)^2}{A} \pm a_p A^{-3/4}, \quad (1)$$

where $A = Z + N$ is the mass number and a_v , a_s , a_c , a_{sym} , and a_p the volume, surface, Coulomb, symmetry energy, and pairing coefficients, respectively. The symmetry energy, $a_{\text{sym}}(A)(N-Z)^2/A$, reduces the total binding energy $B(Z, A)$ of a nucleus as the neutron-proton asymmetry becomes larger, i.e. for $N \gg Z$, yields the typical negative slope of the binding energy curve (Krane 1991) for $A > 62$, and it is divided by A to reduce its importance for heavy nuclei. Its convergence for heavy nuclei establishes the frontiers of the neutron

drip line for particle-unbound nuclei and eventually leads to the disappearance of protons at extreme nuclear densities (Kutschera 1994).

Furthermore, $a_{\text{sym}}(A)$ is relevant to understanding neutron skins (Piekarewicz et al. 2012), the effect of three-nucleon forces (Hebel & Schwenk 2014) and – through the equation of state (EoS) – supernovae cores, neutron stars, and binary mergers (Steiner et al. 2005; Lattimer 2014; Pearson et al. 2014). The latter is the first observationally confirmed astrophysical site where heavy elements are created through the rapid neutron-capture or *r*-process (Gorieli 2003; Cowan et al. 2021). The identification of heavy elements in neutron star mergers is supported by the infrared afterglow from the kilonova AT2017gfo (Metzger 2017) – only understood by the opacities of heavy nuclei – as well as blueshifted Sr II absorption lines (Watson et al. 2019), following the expansion speed of the ejecta gas at $v = 0.1$ –0.3 c . An alternative interpretation that may cause a similar spectral feature to the Sr II lines is provided by the neutral Helium (He I) absorption line, expected from the α -rich freezeout of neutron-rich ejecta (Perego et al. 2022; Tarumi et al. 2023).

The universality of the *r*-process for the heavy elements with $56 < Z < 90$ is further inferred from the similar abundance patterns

* E-mail: jnorce@uwc.ac.za (JNO); dey.balaram@gmail.com (BD); deepak.pandit@vecc.gov.in (DP)

observed in both extremely metal-poor stars and the Sun (Christlieb et al. 2002; Sneden, Cowan & Gallino 2008; Frebel 2018; Kajino et al. 2019). Scatter from the scaled solar abundance pattern is observed for light elements with $Z \approx 40$ and the heaviest long-lived thorium and uranium, which formed earlier in older metal-poor stars. Further scatter in elements with $Z > 70$ could arise from observational uncertainties (Frebel 2018). Other potential sources of heavy elements involve different types of supernova: magneto-rotational driven supernovae (Reichert et al. 2021), collapsars (Siegel, Barnes & Metzger 2019) – the supernova-triggering collapse of rapidly rotating massive stars – and type-II supernova (Goriely 2003), which need to be considered in order to explain all neutron-capture abundances (Qian 2000; Aoki et al. 2005). Moreover, the intermediate neutron-capture process seems to be the only one capable of explaining unusual abundance patterns in carbon enhanced metal poor stars (Hempel et al. 2016) and Sakurai’s object (Herwig et al. 2011). It is presently not clear whether the intermediate neutron-capture process also contributed to the solar-system abundances.

Among all nuclear properties (e.g. atomic masses, photon-strength functions, level densities, and reaction rates), atomic masses are the key ingredient for the calculations of all other theoretical quantities involved in r -process simulations (Goriely & Arnould 1992; Sun et al. 2008; Van Schelt et al. 2013; Mumpower, Surman & Aprahamian 2015c). Albeit atomic-mass-model predictions exhibit significant variations when extrapolating from the known nuclei to the unknown neutron-rich exotic nuclides (Mumpower et al. 2015c), recent microscopic density functional calculations with different interactions suggest that such uncertainties could be substantially reduced with a better understanding of the nuclear symmetry energy (Wang & Chen 2015). Although there may be different astrophysical sites for the r -process nucleosynthesis, we intrinsically investigate the potential universality of elemental abundances from available nuclear properties. Particularly, by confining the neutron drip line with the nuclear symmetry energy extracted from available nuclear data at different temperatures T ; namely, photoabsorption cross sections, binding energies, and giant dipole resonances (GDRs). Such observables are sensitive to nuclear masses and constrain the crust and outer core of the neutron star EoS (Neill et al. 2023).

2 SYMMETRY ENERGY FOR GROUND STATES

Generally, $a_{\text{sym}}(A)$ is parametrized using the leptodermous approximation of Myers and Swiatecki, where $A^{-1/3} \ll 1$ (Myers & Swiatecki 1969),

$$a_{\text{sym}}(A) = S_v \left(1 - \frac{S_s}{S_v} A^{-1/3} \right), \quad (2)$$

which considers the modification of the volume symmetry energy, S_v , by the surface symmetry energy S_s . The leptodermous parametrization arises as a result of nuclear surface effects being localized within the liquid-drop model (Möller et al. 2019) and was chosen on the account of its better fit to the masses of isobaric nuclei (Tian et al. 2014). Constraints on these parameters have been investigated using experimental and theoretical information concerning properties of ground states, i.e. at $T = 0$ MeV (Trippa, Colò & Vigezzi 2008; Lattimer & Lim 2013).

The GDR represents the main contribution to the absorption and emission of electromagnetic radiation (photons) in nuclei (Berman & Fultz 1975). Macroscopically, the dynamics of this quantum collective excitation is characterized by the inter-penetrating motion of proton and neutron fluids out of phase (Migdal 1945), which results from the density-dependent symmetry energy, $a_{\text{sym}}(A)(\rho_N - \rho_Z)^2/\rho$,

acting as a restoring force (Berman & Fultz 1975); where ρ_N , ρ_Z , and $\rho = \rho_N + \rho_Z$ are the neutron, proton, and total density, respectively, which spread uniformly throughout the nucleus. The complementary microscopic interpretation involves a shell-model (SM) representation as a system of independent nucleons plus the residual interaction (Wilkinson 1956; Balashov 1962) or one-particle-one-hole excitations within e.g. the quasi-particle random phase approximation (Ishkhanov & Kapitonov 2021).

The ratio of the induced dipole moment to an applied constant electric field yields the static nuclear polarizability, α . Using the hydrodynamic model and assuming inter-penetrating proton and neutron fluids with a well-defined nuclear surface of radius $R = r_0 A^{1/3}$ fm and ρ_Z as the potential energy of the liquid drop, Migdal (Migdal 1945) obtains the following relation between the static nuclear polarizability, α , and a_{sym} :

$$\alpha = \frac{e^2 R^2 A}{40 a_{\text{sym}}} = 2.25 \times 10^{-3} A^{5/3} \text{fm}^3, \quad (3)$$

where $r_0 = 1.2$ fm, $e^2 = 1.44$ MeV fm in the c.g.s. system, and a constant value of $a_{\text{sym}} = 23$ MeV was utilized.

Alternatively, α can be calculated for the ground states of nuclei using second-order perturbation theory (Levinger 1960) following the sum rule:

$$\alpha = 2e^2 \sum_n \frac{\langle i \| \hat{E}1 \| n \rangle \langle n \| \hat{E}1 \| i \rangle}{E_\gamma} \quad (4)$$

$$= \frac{e^2 \hbar^2}{M} \sum_n \frac{f_{in}}{E_\gamma^2} = \frac{\hbar c}{2\pi^2} \int_0^\infty \frac{\sigma_{\text{total}}(E_\gamma)}{E_\gamma^2} dE_\gamma \quad (5)$$

$$= \frac{\hbar c}{2\pi^2} \sigma_{-2}, \quad (6)$$

where E_γ is the γ -ray energy corresponding to a transition connecting the ground state $|i\rangle$ and an excited state $|n\rangle$, M the nucleon mass, f_{in} the dimensionless oscillator strength for $E1$ transitions (Levinger 1960), and σ_{-2} the second moment of the total electric-dipole photo-absorption cross section,

$$\sigma_{-2} = \int_0^\infty \frac{\sigma_{\text{total}}(E_\gamma)}{E_\gamma^2} dE_\gamma, \quad (7)$$

where $\sigma_{\text{total}}(E_\gamma)$ is the total photo-absorption cross section, which generally includes $(\gamma, n) + (\gamma, pn) + (\gamma, 2n) + (\gamma, 3n)$ photoneutron and available photoproton and photofission cross sections (Kawano et al. 2020), in competition in the GDR region (Bergère 1977; Snover 1986). By comparing equations (3) and (6), a mass-dependent symmetry energy, $a_{\text{sym}}(A)$, is extracted in units of MeV,

$$a_{\text{sym}}(A) = \frac{e^2 R^2 \pi^2 A}{20 \hbar c \sigma_{-2}} \approx 5.2 \times 10^{-3} \frac{A^{5/3}}{\sigma_{-2}}. \quad (8)$$

Empirical evaluations reveal that σ_{-2} can also be approximated by $\sigma_{-2} = 2.4\kappa A^{5/3}$, where the dipole polarizability parameter κ measures GDR deviations between experimental and hydrodynamic model predictions (Orce 2020).

Fig. 1 shows the distribution of $a_{\text{sym}}(A)$ for the ground state of stable isotopes, along the nuclear landscape, determined from empirical σ_{-2} values. Data include all available emission channels. The contribution of (γ, p) cross sections are evident in light nuclei, which significantly reduces the symmetry energy. For heavy nuclei, (γ, n) cross sections are dominant because of the higher Coulomb barrier. A fit to the data using equation (2) (solid line) yields $a_{\text{sym}}(A) = 31.1(13)(1 - 1.1(1)A^{-1/3})$ MeV, where the standard deviation of the best-fit parameters were determined using automatic differentiation

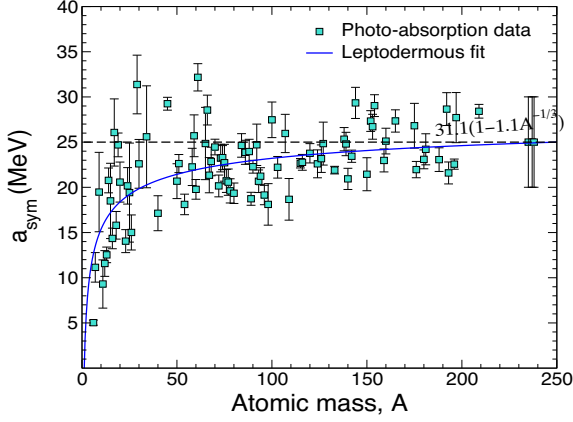


Figure 1. Symmetry energy coefficient, $a_{\text{sym}}(A)$, of finite nuclei as a function of mass number A extracted from the experimental σ_{-2} values extracted from available photoabsorption cross sections (McLane 2001; Data Data), as given in equation (8) and fitted (solid line) by equation (2).

(Neidinger 2010). Unfortunately, (γ, p) cross-section data are very scarce, which directly affects the $a_{\text{sym}}(A)$ trend for $A \lesssim 70$ in Fig. 1.

In addition, Tian and co-workers determined $a_{\text{sym}}(A) = 28.32(1 - 1.27A^{-1/3})$ MeV from a global fit to the binding energies of isobaric nuclei with mass number $A \geq 10$ (Tian et al. 2014) – extracted from the 2012 atomic mass evaluation (AME; Audi et al. 2014) – with $S_v \approx 28.32$ MeV being the bulk symmetry energy coefficient and $\frac{S_s}{S_v} \approx 1.27$ the surface-to-volume ratio. Similar coefficients are calculated in Danielewicz (2003) and Steiner et al. (2005). Within this approach, the extraction of $a_{\text{sym}}(A)$ only depends on the Coulomb energy term in the SEMF and shell effects (Koura et al. 2005) – which are both included (Tian et al. 2014) – and $a_{\text{sym}}(A)$ presents a maximum energy around 23 MeV. This description of $a_{\text{sym}}(A)$ has been used to explain the enhanced σ_{-2} values observed for low-mass nuclei (Orce 2015).

The symmetry energy $a_{\text{sym}}(A)$ is the fundamental parameter that characterizes the energy of the GDR, E_{GDR} , within the Steinwedel–Jensen (SJ) model of proton and neutron compressible fluids moving within the rigid surface of the nucleus (Steinwedel, Jensen & Jensen 1950). Danos improved the SJ model by including the GDR width, Γ_{GDR} (Danos 1958; Berman & Fultz 1975) in the second-sound hydrodynamic model (Danos 1958; Berman & Fultz 1975), where E_{GDR} and Γ_{GDR} are related to $a_{\text{sym}}(A)$ as (Bergère 1977),

$$a_{\text{sym}}(A) = \frac{MA^2}{8h^2K^2NZ} \frac{E_{\text{GDR}}^2}{1 - \left(\frac{\Gamma_{\text{GDR}}}{2E_{\text{GDR}}}\right)^2} \approx 1 \times 10^{-3} \left(\frac{A^{8/3}}{NZ}\right) \frac{E_{\text{GDR}}^2}{1 - \left(\frac{\Gamma_{\text{GDR}}}{2E_{\text{GDR}}}\right)^2}, \quad (9)$$

where K is the real eigenvalue of $\nabla^2 \rho_z + K^2 \rho_z = 0$, with the boundary condition $(\hat{\mathbf{n}} \cdot \nabla \rho_z)_{\text{surface}} = 0$, and has a value of $KR = 2.082$ for a spherical nucleus (Rayleigh 1896). For quadrupole deformed nuclei with an eccentricity of $a^2 - b^2 = \epsilon R^2$, where a and b are the half axes and ϵ the deformation parameter, the GDR lineshape splits into two peaks with similar values of Ka and $Kb \approx 2.08$ (Danos 1958). For deformed nuclei, we estimate a similar equation to equation (9), but using the average centroid energy and the full width at half-maximum of the total Lorentzian (see e.g. Gaardhøje, Bruce & Herskind 1988).

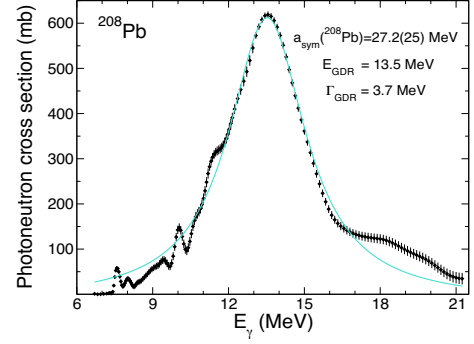


Figure 2. A Lorentzian fit to GDR data extracted for ^{208}Pb (McLane 2001; Data).

Uncertainties in the quoted values arise from the error propagation of equation (9).

The GDR cross-section data for each nucleus were obtained from the EXFOR and ENDF data (McLane 2001; Data) and fitted with one or two Lorentzian curves to extract E_{GDR} and Γ_{GDR} , as shown e.g. in Fig. 2 for ^{208}Pb . The data set for each nucleus was selected based on the number of data points, experimental method, and energy range. In this work, the maximum integrated γ -ray energy, E_{γ}^{max} , was in the range 20–50 MeV therefore excluding contributions resulting from high energy effects such as pion exchange and other meson resonances. The resulting distribution of $a_{\text{sym}}(A)$ is shown in the left-hand panel of Fig. 3, which converges at approximately 27 MeV for heavy nuclei. It is reassuring that the two methods based on photoabsorption cross-section data – namely $a_{\text{sym}}(A)$ extracted from σ_{-2} values and parameters of GDRs built on ground states – present similar trends.

Data obtained from GDR parameters at $T = 0$ can also be fitted to equation (2), which yields $a_{\text{sym}}(A) = 35.3(7)(1 - 1.58(5)A^{-1/3})$ MeV (red solid band in Fig. 3). Larger values of $S_v = 42.8$ MeV and $S_s = 89.9$ MeV were determined by Berman using equation (9) for 29 nuclei ranging from $A = 75$ to 209 (Berman 1973). Furthermore, Berman argued that assuming a surface binding energy coefficient of $a_s = 20$ MeV in the SEMF, the large symmetry to surface energy ratio, $S_s/a_s = 4.5$, favours – as a result of a steeper slope of the binding energy curve for heavy nuclei – a close-in neutron drip line for heavy elements; hence, constraining the reaction network that produces heavy elements by the r -process in neutron mergers and supernovae. Using our value of $S_s = 55.8$ MeV and $a_s = 20$ MeV, a more standard ratio of $S_s/a_s = 2.8$ is determined (Orce 2016). Slightly smaller values of $a_s \approx 17$ MeV are also found in the literature (Krane 1991; Danielewicz 2003), yielding $S_s/a_s = 2.7$.

3 SYMMETRY ENERGY FOR EXCITED STATES

Furthermore, it is interesting to investigate the behavior of $a_{\text{sym}}(A)$ using the available information on GDRs built on excited states, below the critical temperatures and spins where the GDR width starts broadening; i.e. for moderate average temperatures of $T \lesssim T_c = 0.7 + 37.5/A$ MeV and spins I below the critical angular momentum $I \lesssim I_c = 0.6A^{5/6}$ (Kusnezov, Alhassid & Snover 1998). In fact, similar centroid energies, $E_{\text{GDR}}^{\text{exc}}$, and resonance strengths, $S_{\text{GDR}}^{\text{exc}}$ – relative to the Thomas–Reiche–Kuhn $E1$ sum rule (Levinger 1960) – to those found for the ground-state counterparts (Snover 1986; Gaardhøje 1992) indicate a common physical origin for all GDRs, in concordance with the Brink–Axel hypothesis that assumes that a GDR can be built on every state in a nucleus (Brink 1955; Axel 1962).

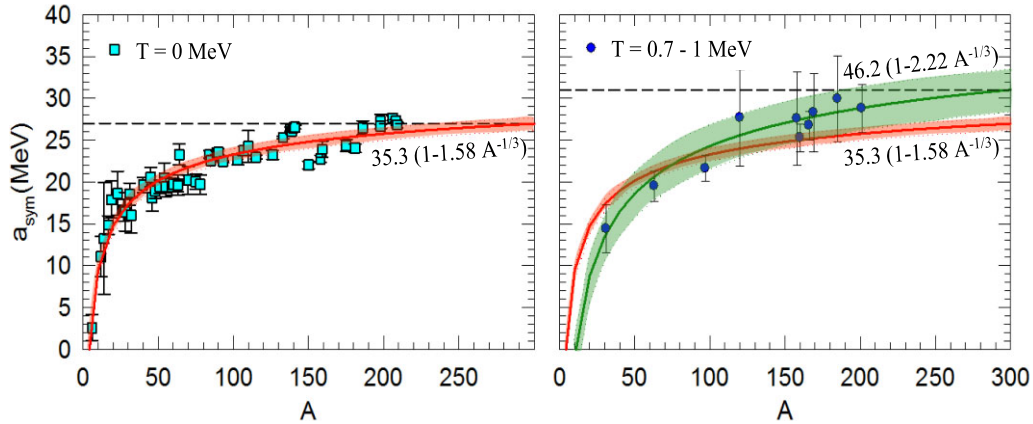


Figure 3. Symmetry energy coefficient, $a_{\text{sym}}(A)$, of finite nuclei as a function of mass number A extracted from GDRs built on ground states ($T = 0$; left-hand panel) and excited states ($T = 0.7\text{--}1$ MeV; right-hand panel) using equation (9).

The validity of the Brink–Axel hypothesis remain to be verified for nuclei far from stability.

Applying again equation (9), the right-hand panel of Fig. 3 shows $a_{\text{sym}}(A)$ values for GDRs built on excited states in slightly-deformed nuclei ^{31}P (Mondal et al. 2018), ^{63}Cu (Kicińska-Habior et al. 1987), ^{97}Tc (Dey et al. 2014), ^{120}Sn (Heckman et al. 2003), and ^{201}Tl (Pandit et al. 2012), as well as for well-deformed nuclei in the $A \approx 160\text{--}180$ mass region ($^{158, 160, 166}\text{Er}$, ^{169}Tm , and ^{185}Re ; Gossett et al. 1985; Gaardhøje et al. 1988; Pandit et al. 2021). With an average temperature between $T \approx 0.7$ and 1.0 MeV and below J_c , these nuclei were selected to investigate the symmetry energy at temperatures relevant to the r -process nucleosynthesis. Surprisingly, $a_{\text{sym}}(A)$ values for heavy nuclei are relatively larger than previously observed at $T = 0$ MeV. A fit to the data using equation (2) (green solid line in Fig. 3) yields $a_{\text{sym}}(A) = 46.2(2.4)(1 - 2.22(14)A^{-1/3})$ MeV, converging at $a_{\text{sym}} \approx 31$ MeV for heavy nuclei. Two bands showing the loci limits of the two fitting curves at $T = 0$ and $T \approx 0.7\text{--}1$ MeV are shown for comparison. Such a distinct behaviour could clearly affect nucleosynthesis of heavy elements via the r -process during the cooling down of the ejecta.

4 DISCUSSION AND CONCLUSIONS

Lighter or heavier seed nuclei are generally produced depending on the density and temperature of the ejecta gas. Assuming nuclear-statistical equilibrium – when forward and reverse reactions are balanced – abundances follow a Maxwell-Boltzmann distribution where lighter seed nuclei are favoured at very high temperatures ($\propto kT^{-3/2(A-1)}$) and heavier nuclei are favoured at very high densities ($\propto \rho^A$), as those found in the ejecta of neutron-star mergers (Thielemann et al. 2017). At temperatures below $T = 1$ MeV (or 1.2×10^{10} K), seed nuclei are produced before charge reactions freeze out – impeded by the Coulomb barrier – at about $T \approx 0.5$ MeV (or 5×10^9 K). Thereafter, heavy nuclei are produced through subsequent neutron capture until neutron reactions freeze out – as neutrons are finally consumed – at a few 10^8 K.

Our work may not be sensitive to the lower temperatures occurring during neutron capture in neutron-star mergers, which likely range from $T \approx 0.5 \times 10^8$ K (Goriely, Bauswein & Janka 2011) to $T \approx 5 \times 10^9$ K (Wu et al. 2016); i.e. in the range from $T \approx 0.04$ to 0.43 MeV, respectively. Nevertheless, Fig. 4 shows that the symmetry energy does not change with temperature in the $[0.74, 1.3]$

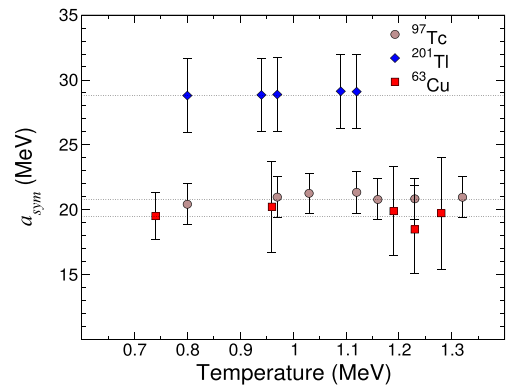


Figure 4. Symmetry energy coefficient, $a_{\text{sym}}(A)$ extracted for ^{63}Cu , ^{97}Tc , and ^{201}Tl as a function of temperature, T . A similar constant behaviour is observed for other nuclei. The horizontal dotted lines are shown as a reference.

MeV range, which suggests that this relation could still hold at lower temperatures down to the lower limits for the waiting point approximation, i.e. for $T \gtrsim 1$ GK or $T \gtrsim 0.1$ MeV, where neutron captures become balanced by high-energy photons from neutron photodisintegrations (Cameron, Cowan & Truran 1983).

In the current work, we notice a slight increase of 3–5 per cent in the centroid energy at $T \approx 0.7\text{--}1$ MeV as compared with the ground-state values for nearly-spherical ^{120}Sn (Heckman et al. 2003), ^{208}Pb (Baumann et al. 1998), and ^{201}Tl (Pandit et al. 2012) nuclei as well as for the deformed nuclei in the $A = 160\text{--}180$ mass region (Gossett et al. 1985; Gaardhøje et al. 1988; Pandit et al. 2021). Although such an increase is within the experimental errors, it leads to a distinct systematic behaviour, as shown in the right-hand panel of Fig. 3. In fact, the temperature dependence of the symmetry energy has been studied within the liquid-drop and Fermi gas models (Bortignon, Bracco & Broglia 2019), where an effective nucleon mass – the so-called ‘ w ’ mass – is introduced to account for the non-locality of the Hartree–Fock potential. Such an increase in the symmetry energy may therefore arise from the change in the effective mass of the nucleon, which decreases as T increases in the temperature interval $0 < T < 1$ MeV (Donati et al. 1994). This leads to an increase in the centroid energy of the GDR, which results in an increase of the symmetry energy of medium and heavy mass nuclei by approximately 8 per cent at $T \approx 1$ MeV (Donati et al. 1994).

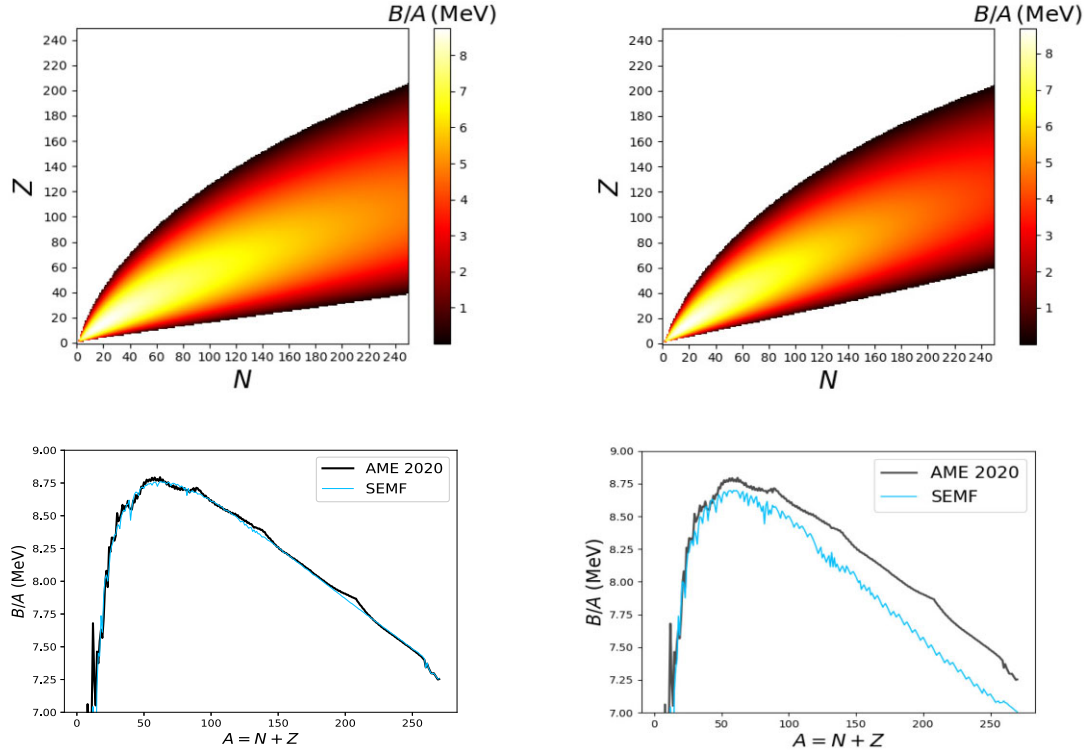


Figure 5. Nuclear charts (top panels) and binding energy curves (bottom panels) showing average binding energies per nucleon using the Bethe–Weizsäcker SEMF for $a_{\text{sym}} = 23.7$ (Rohlf 1994) MeV (left) and $a_{\text{sym}} = 31$ MeV (right). Atomic masses in the bottom panels are extracted from the 2020 AME (Wang et al. 2021).

In contrast, Monte Carlo SM calculations do not predict such a generic increase of the symmetry energy coefficient as a function of temperature for $T < 1$ MeV (Dean et al. 1995), which clearly demands further mean-field calculations.

The effect from a larger symmetry energy at $T \approx 0.7$ – 1 MeV is illustrated in Fig. 5, which shows the corresponding nuclear charts (top) and binding energy curves (bottom) using $a_{\text{sym}} = 23.7$ MeV (left) (Rohlf 1994) and 31 MeV (right), respectively. The nuclear chart determined using $a_{\text{sym}} = 31$ MeV illustrates a substantial close-in of the neutron drip line, as a result of the decreasing binding energy per nucleon in neutron-rich nuclei. For instance, the drip line closes in from ^{254}Pt to ^{216}Pt for $a_{\text{sym}} = 23.7$ and 31 MeV, respectively. Fig. 6 shows the respective neutron drip lines without shell effects and clearly illustrates the effect of an enhanced symmetry energy in the production of heavy elements, which constrains exotic r -process paths far away from the line of stability, and plausibly explains the universality of r -process abundances inferred from the observation of extremely metal-poor stars and our Sun.

Consequently, such an increase in the symmetry energy leads to the reduction of radiative neutron capture rates as neutron-rich nuclei become less bound. The corresponding change in the capture cross section has been calculated using TALYS (Koning, Hilaire & Duijvestijn 2007) and EMPIRE (Herman et al. 2007) codes for nuclides close to our predictive neutron drip line, by changing only the mass excess with standard input parameters. Other inputs such as level densities and photon strength functions are unknown far from stability. Both codes yield similar results with a reduction of the neutron-capture cross section by a factor of the order of 10^2 in the $A \approx 200$ mass region relevant to the r -process. More detailed calculations will be presented in a separate manuscript. These findings support

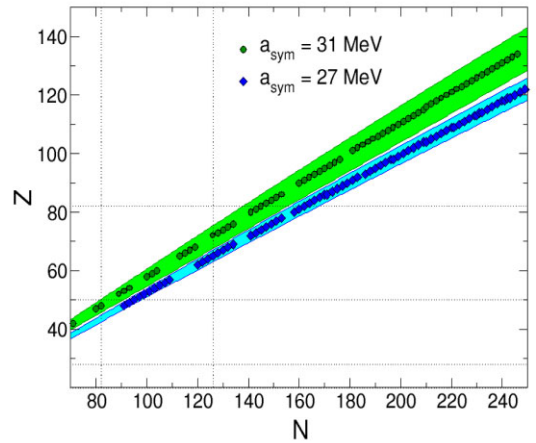


Figure 6. Neutron drip lines predicted at symmetry energy coefficients of $a_{\text{sym}} = 27$ (diamonds) and 31 MeV (circles). Dotted lines indicate the proton and neutron magic numbers.

the rapid drop of the neutron capture rates at increasing neutron excesses inferred from Goriely’s microscopic calculations at $T = 1.5 \times 10^9$ K (Goriely 2003). As nicely put by Goriely: ‘the so-called ‘universality’ of the r -process abundances (as inferred from spectroscopic observation of ultra-metal-poor stars) could possibly be explained by the rapid drop of the neutron capture rates at increasing neutron excesses (which constrains the r -process flow to remain in the narrow region of the nuclear chart characterized by low β half-lives and large neutron capture rates)’.

Further, there are modified versions of the SEMF which consider updated parameters (Ankita & Suthar 2016) or isospin effects (Sakinah & Sulistyani 2019), and also more sophisticated mass models with stronger physics foundations, which are typically used in r -process calculations (Duflo & Zuker 1995; Geng, Toki & Meng 2005; Pearson et al. 2014; Wang et al. 2014; Möller et al. 2016). For instance, the microscopic–macroscopic Weizsäcker–Skyrme (WS; Wang et al. 2014) and Duflo–Zuker (Duflo & Zuker 1995) models present the lowest rms deviations of about 300 keV with respect to the available mass data. Nevertheless, as pointed out by Mumpower and collaborators (Mumpower et al. 2015c), only a reduction of global rms errors below 100 keV may allow for accurate r -process predictions and differentiation between model predictions, which can range orders of magnitude. The variability arise from mass variations of unmeasured nuclei, and it is large enough to prevent the distinction between mass model extrapolations for given astrophysical conditions. In particular, sensitivity studies of individual nuclear masses (Mumpower et al. 2016) yields a variation of up to an order of magnitude local change in the final abundance pattern produced in an r -process simulation; a situation which is slightly improved when using parameters of energy density functionals with full correlations contained in the model (Sprouse et al. 2020), although still remains the one order of magnitude variation, specially for nuclei around the closed shells. A similar study by Jiang and co-workers (Jiang, Wu & Zhao 2021) indicates the lack of a regular relation between the r -process abundance deviations and the rms deviations of masses, but also infer – from systematic sensitivity studies – that a mass uncertainty of ± 0.5 MeV would yield an abundance uncertainty of a factor around 2.5.

Despite the lack of precise mass models with rms < 100 keV, we have performed sensitivity studies of r -process nucleosynthesis using the r -process code SiRop (Kostka et al. 2014; Shand 2016) within the waiting point approximation. We considered the Hartree–Fock–Bogoliubov (HFB-21; Goriely, Chamel & Pearson 2009; Pearson et al. 2014; Goriely, Chamel & Pearson 2016) and the finite-range droplet (FRDM; Möller et al. 2016) mass models using the r -process code SiRop (Kostka et al. 2014; Shand 2016). The FRDM considers the combination of the finite-range droplet macroscopic model and the folded-Yukawa single-particle microscopic model, and uses a similar symmetry energy constant J , which relates to $a_{\text{sym}}(A)$ as (Myers & Swiatecki 1969; Centelles et al. 2009),

$$a_{\text{sym}}(A) = \frac{J}{1 + \frac{9J}{4Q} A^{-1/3}}, \quad (10)$$

where $Q = 28.72$ MeV is the surface stiffness and $J = 32.3$ MeV (Möller et al. 2016) for bulk matter is larger than $a_{\text{sym}}(A)$ for finite nuclei. Similar J values are obtained with the HFB models – which result in a favourable bulk value of $J = 30$ MeV when compared with observations of neutron stars (Pearson et al. 2014; Goriely et al. 2016) – in agreement with experimental constraints (Tsang et al. 2012; Roca-Maza et al. 2013).

As revealed by previous sensitivity studies, atomic masses of nuclei near closed-shells and in the rare-earth region 10–20 neutrons from stability present a more substantial impact on abundance predictions for different neutron star merger r -process scenarios (Surman et al. 2014; Mumpower et al. 2015a, b, 2016; Martin et al. 2016). Here, we have selected nuclei in the mass $A \approx 200$ –220 region (e.g. ^{204}Pt , ^{220}Pt) as our testing ground for r -process network calculations using a baseline with $T = 3$ GK as the initial temperature, neutron density $\rho = \frac{\rho_0}{(1+t/2\tau)^2}$ with $\rho_0 = 10^{11}$ g cm $^{-3}$ and $\tau = 0.1$ s (Shand et al. 2016, 2017). For each isotope the simulation was run assuming an increase in the isotopic mass by a percentage

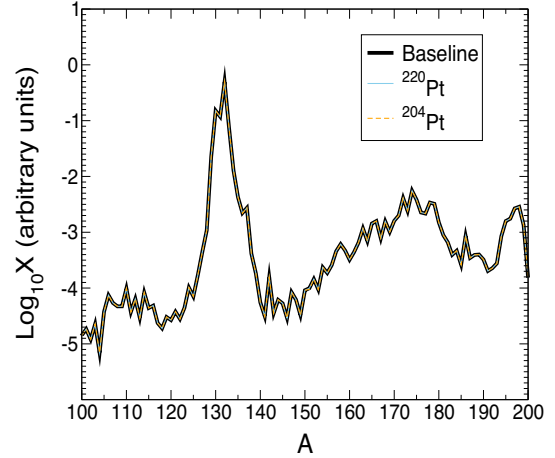


Figure 7. Abundance pattern in the r -process simulation showing the baseline versus two single mass changes for ^{204}Pt and ^{220}Pt . The atomic mass was increased by approximately 0.05 per cent and 0.07 per cent, respectively, corresponding to a change in the symmetry energy from $a_{\text{sym}} = 23$ to 31 MeV.

corresponding to the change in $a_{\text{sym}}(A)$. For instance, an additional 0.05 per cent in the atomic mass of ^{204}Pt arises from changing $a_{\text{sym}}(A)$ from 23 to 31 MeV ($a_{\text{sym}}(A) = 23$ MeV corresponds to $J = 32.3$ MeV and $a_{\text{sym}}(A) = 31$ MeV to $J = 51$ MeV). Although astrophysical environments present different abundance patterns that depend on the initial conditions, changes in the atomic mass of single isotopes due to different $a_{\text{sym}}(A)$ values do not produce – as shown in Fig. 7 – an apparent change in the abundance pattern.

This is probably not surprising as sensitivity predictions from the FRDM have been compared with the Duflo–Zuker, WS, and HFB-17 mass models in previous sensitivity studies, yielding similar results for every heavy element isotopic chain where atomic masses had been measured, but presenting large disagreements away from known values – in excess of 1 MeV – as models extend towards the drip line (see e.g. fig. 1 in Mumpower et al. 2015a). More detailed r -process network calculations are under way, including multiple mass changes for different isotopic and/or isotonic chains and gradually moving away from the stability line, as sensitivity studies rapidly lose their predictive power further away from the stability. The results will be presented in a separate manuscript.

Finally, more experimental data regarding neutron-capture rates using novel techniques (Larsen et al. 2019) and GDRs built on excited states with $T \lesssim 0.7$ MeV are crucially needed in order to elucidate the nature of the symmetry energy as a function of temperature. This avenue of research can be pursued with the inelastic scattering of α particles (Ramakrishnan et al. 1996; Baumann et al. 1998) and modern gamma-ray spectrometers such as the GAMKA array at iThemba LABS in South Africa (Orce & Ntshangase 2021). It should be noted that the universal abundance pattern for heavy elements between Ba and Pb suggested in this work assumes the validity of the SEMF, the Brink–Axel hypothesis and the temperature dependence of the symmetry energy, in agreement with available data for stable or close-to-stable nuclei. These assumptions may not be valid for exotic nuclides close to the neutron drip line, where the r -process occurs. In fact, recent finite temperature HFB calculations (Yüksel 2021) suggest that some neutron unbound nuclei at $T = 0$ may become bound at high excitation energies, which yields the opposite effect, i.e. the opening of the neutron drip line. In addition, dynamical effects rather than those affecting the location of the drip line may disrupt the

r-process universality. For instance, late-time neutron-captures that may compete with β -decays and alter the neutron density as the *r*-process decays back to stability, especially affecting the abundance of closed-shell nuclei (Surman et al. 2009; Vescovi et al. 2022). Modern radioactive ion beam facilities such as the Facility for Rare Isotope Beams at Michigan State University will explore the limits of the nuclear landscape (Neufcourt et al. 2020) and may support or refute our ideas.

ACKNOWLEDGEMENTS

The authors would like to thank Matthew Mumpower, Nicholas Chamel, Nicholas Koning, and Rachid Ouyed for physics discussions and support related to *r*-process network calculations.

DATA AVAILABILITY

The data underlying this article are available from online sources at the nuclear reaction databases: EXFOR: Experimental Nuclear Reaction Data, <https://www-nds.iaea.org/exfor/exfor.htm>, ENDF: Evaluated Nuclear Data File, <https://www-nds.iaea.org/exfor/endl.htm>, and Atomic Masses at AMDC: <https://www-nds.iaea.org/amdc/>.

REFERENCES

- Ankita, Suthar B., 2016, in AIP Conference Proceedings. p. 20024
 Aoki W. et al., 2005, *ApJ*, 632, 611
 Audi G., Wang M., Wapstra A. H., Kondev F. G., MacCormick M., Xu X., 2014, *Nucl. Data Sheets*, 120, 1
 Axel P., 1962, *Phys. Rev.*, 126, 671
 Balashov V. V., 1962, *Zh. Eksp. Teor. Fiz.*, 42, 275
 Baumann T. et al., 1998, *Nucl. Phys. A*, 635, 428
 Bergère R., 1977, *Lect. Notes Phys.*, 61, 1
 Berman B. L., Fultz S., 1975, *Rev. Mod. Phys.*, 47, 713
 Berman B. L., 1973, Proceedings of the International Conference on Photonuclear Reactions and Applications. Pacific Grove, California
 Bethe H. A., Bacher R. F., 1936, *Rev. Mod. Phys.*, 8, 82
 Bortignon P. F., Bracco A., Broglia R. A., 2019, Giant Resonances: Nuclear Structure at Finite Temperature. Taylor & Francis
 Brink D. M., 1955, PhD thesis, University of Oxford
 Cameron A. G. W., Cowan J. J., Truran J. W., 1983, *Astrophys. Space Sci.*, 91, 235
 Centelles M., Roca-Maza X., Vinas X., Warda M., 2009, *Phys. Rev. Lett.*, 102, 122502
 Christlieb N. et al., 2002, *Nature*, 419, 904
 Cowan J. J., Sneden C., Lawler J. E., Aprahamian A., Wiescher M., Langanke K., Martínez-Pinedo G., Thielemann F.-K., 2021, *Rev. Mod. Phys.*, 93, 15002
 Danielewicz P., 2003, *Nucl. Phys. A*, 727, 233
 Danos M., 1958, *Nucl. Phys.*, 5, 23
 EXFOR Data, <https://www-nds.iaea.org/exfor>
 Dean D. J., Koonin S. E., Langanke K., Radha P. B., 1995, *Phys. Lett. B*, 356, 429
 Dey B. et al., 2014, *Phys. Lett. B*, 731, 92
 Donati P., Pizzochero P. M., Bortignon P. F., Broglia R. A., 1994, *Phys. Rev. Lett.*, 72, 2835
 Dufflo J., Zuker A. P., 1995, *Phys. Rev. C*, 52, R23
 Frebel A., 2018, *Annu. Rev. Nucl. Part. Sci.*, 68, 237
 Gaardhoje J. J., 1992, *Annu. Rev. Nucl. Part. Sci.*, 42, 483
 Gaardhoje J. J., Bruce A. M., Herskind B., 1988, *Nucl. Phys. A*, 482, 121
 Geng L., Toki H., Meng J., 2005, *Prog. Theor. Phys.*, 113, 785
 Goriely S., 2003, *Nucl. Phys. A*, 718, 287
 Goriely S., Arnould M., 1992, *Astron. Astrophys.*, 262, 73
 Goriely S., Chamel N., Pearson J. M., 2009, *Phys. Rev. Lett.*, 102, 152503
 Goriely S., Bauswein A., Janka H.-T., 2011, *ApJ*, 738, L32

- Goriely S., Chamel N., Pearson J. M., 2016, *Phys. Rev. C*, 93, 34337
 Gossett C. A., Snover K. A., Behr J. A., Feldman G., Osborne J. L., 1985, *Phys. Rev. Lett.*, 54, 1486
 Hampel M., Stancliffe R. J., Lugaro M., Meyer B. S., 2016, *ApJ*, 831, 171
 Hebel K., Schwenk A., 2014, *Eur. Phys. J. A*, 50, 1
 Heckman P. et al., 2003, *Phys. Lett. B*, 555, 43
 Herman M., Capote R., Carlson B., Obložinský P., Sin M., Trkov A., Wienke H., Zerkin V., 2007, *Nucl. Data Sheets*, 108, 2655
 Herwig F., Pignatari M., Woodward P. R., Porter D. H., Rockefeller G., Fryer C. L., Bennett M., Hirschi R., 2011, *ApJ*, 727, 89
 Ishkhanov B. S., Kapitonov I. M., 2021, *Phys. Usp.*, 64, 141
 Jiang X.-F., Wu X.-H., Zhao P.-W., 2021, *ApJ*, 915, 29
 Kajino T., Aoki W., Balantekin A. B., Diehl R., Famiano M. A., Mathews G. J., 2019, *Prog. Part. Nucl. Phys.*, 107, 109
 Kawano T. et al., 2020, *Nucl. Data Sheets*, 163, 109
 Kicińska-Habior M., Snover K. A., Gossett C. A., Behr J. A., Feldman G., Glatzel H. K., Gundlach J. H., Garman E. F., 1987, *Phys. Rev. C*, 36, 612
 Koning A. J., Hilaire S., Duijvestijn M. C., 2007, in International Conference on Nuclear Data for Science and Technology. EDP Sciences, p. 211
 Kostka M., Koning N., Shand Z., Ouyed R., Jaikumar P., 2014, *Astron. Astrophys.*, 568, A97
 Koura H., Tachibana T., Uno M., Yamada M., 2005, *Prog. Theor. Phys.*, 113, 305
 Krane K. S., 1991, *Introductory Nuclear Physics*. John Wiley and Sons
 Kusnezov D., Alhassid Y., Snover K. A., 1998, *Phys. Rev. Lett.*, 81, 542
 Kutschera M., 1994, *Phys. Lett. B*, 340, 1
 Larsen A.-C., Spyrou A., Liddick S. N., Guttormsen M., 2019, *Prog. Part. Nucl. Phys.*, 107, 69
 Lattimer J. M., 2014, *Nucl. Phys. A*, 928, 276
 Lattimer J. M., Lim Y., 2013, *ApJ*, 771, 51
 Levinger J. S., 1960, *Nuclear Photo-disintegration*. Oxford Univ. Press, Oxford
 McLane V., 2001, Technical Report, ENDF-102 Data Formats and Procedures for the Evaluated Nuclear Data File ENDF-6. Brookhaven National Laboratory. Long Island, New York
 Martin D., Arcones A., Nazarewicz W., Olsen E., 2016, *Phys. Rev. Lett.*, 116, 121101
 Metzger B. D., 2017, *Living Rev. Relativ.*, 20, 1
 Migdal A. B., 1945, *Zh. Eksp. Teor. Fiz.*, 15, 81
 Möller P., Sierk A. J., Ichikawa T., Sagawa H., 2016, *At. Data Nucl. Data Tables*, 109, 1
 Möller P., Mumpower M. R., Kawano T., Myers W. D., 2019, *At. Data Nucl. Data Tables*, 125, 1
 Mondal D. et al., 2018, *Phys. Lett. B*, 784, 423
 Mumpower M. R., Surman R., Fang D. L., Beard M., Aprahamian A., 2015a, *J. Phys. G Nucl. Part. Phys.*, 42, 34027
 Mumpower M. R., Surman R., Fang D. L., Beard M., Möller P., Kawano T., Aprahamian A., 2015b, *Phys. Rev. C*, 92, 35807
 Mumpower M. R., Surman R., Aprahamian A., 2015c, in EPJ Web of Conferences. EDP Sciences, p. 3003
 Mumpower M. R., Surman R., McLaughlin G. C., Aprahamian A., 2016, *Prog. Part. Nucl. Phys.*, 86, 86
 Myers W. D., Swiatecki W. J., 1969, *Ann. Phys.*, 55, 395
 Neidinger R. D., 2010, *SIAM Rev.*, 52, 545
 Neill D., Preston R., Newton W. G., Tsang D., 2023, *Phys. Rev. Lett.*, 130, 112701
 Neufcourt L. et al., 2020, *Phys. Rev. C*, 101, 44307
 Orce J. N., 2015, *Phys. Rev. C*, 91, 64602
 Orce J. N., 2016, Šimkovich F., ed., Proceedings 4th SA-JINR Workshop. JINR, Dubna. p. 64
 Orce J. N., 2020, *Int. J. Mod. Phys. E*, 29, 2030002
 Orce J. N., Ntshangase S., 2021, *Nat. Phys.*, 17, 1187
 Pandit D., Mukhopadhyay S., Pal S., De A., Banerjee S. R., 2012, *Phys. Lett. B*, 713, 434
 Pandit D. et al., 2021, *Phys. Lett. B*, 816, 136173
 Pearson J. M., Chamel N., Fantina A. F., Goriely S., 2014, *Eur. Phys. J. A*, 50, 1

- Perego A. et al., 2022, *ApJ*, 925, 22
- Piekarewicz J., Agrawal B. K., Colo G., Nazarewicz W., Paar N., Reinhard P.-G., Roca-Maza X., Vretenar D., 2012, *Phys. Rev. C*, 85, 41302
- Qian Y. Z., 2000, *ApJ*, 534, L67
- Ramakrishnan E. et al., 1996, *Phys. Rev. Lett.*, 76, 2025
- Rayleigh J. W. S. B., 1896, *The Theory of Sound*. Macmillan and Co., Ltd., New York.
- Reichert M., Obergaulinger M., Eichler M., Aloy M. Á., Arcones A., 2021, *MNRAS*, 501, 5733
- Roca-Maza X. et al., 2013, *Phys. Rev. C*, 88, 24316
- Rohlf J. W., 1994, Wiley: *Modern Physics from Alpha to Z0*-James William Rohlf. John Wiley & Sons Ltd., Hoboken, New Jersey
- Sakinah S. A., Sulistyani E. T., 2019, in *Proceeding International Conference on Science and Engineering*. p. 153
- Shand Z., 2016, Master's thesis, MSc thesis, University of Calgary
- Shand Z., Ouyed A., Koning N., Ouyed R., 2016, *Res. Astron. Astrophys.*, 16, 11
- Shand Z., Ouyed R., Koning N., Dillmann I., Krücken R., Jaikumar P., 2017, preprint (arXiv:1705.00099)
- Siegel D. M., Barnes J., Metzger B. D., 2019, *Nature*, 569, 241
- Snedden C., Cowan J. J., Gallino R., 2008, *Annu. Rev. Astron. Astrophys.*, 46, 241
- Snover K. A., 1986, *Annu. Rev. Nucl. Part. Sci.*, 36, 545
- Sprouse T. M., Perez R. N., Surman R., Mumpower M. R., McLaughlin G. C., Schunck N., 2020, *Phys. Rev. C*, 101, 55803
- Steiner A. W., Prakash M., Lattimer J. M., Ellis P. J., 2005, *Phys. Rep.*, 411, 325
- Steinwedel H., Jensen J. H. D., Jensen P., 1950, *Phys. Rev.*, 79, 1019
- Sun B. et al., 2008, *Phys. Rev. C*, 78, 25806
- Surman R., Beun J., Mclaughlin G. C., Hix W. R., 2009, *Phys. Rev. C*, 79, 45809
- Surman R., Mumpower M. R., Cass J., Bentley I., Aprahamian A., McLaughlin G. C., 2014, in *EPJ Web of Conferences*. EDP Sciences, p. 7024
- Tarumi Y., Hotokezaka K., Domoto N., Tanaka M., 2023, preprint (arXiv:2302.13061)
- Thielemann F. K., Eichler M., Panov I. V., Wehmeyer B., 2017, *Annu. Rev. Nucl. Part. Sci.*, 67, 253
- Tian J., Cui H., Zheng K., Wang N., 2014, *Phys. Rev. C*, 90, 24313
- Trippa L., Colò G., Vigezzi E., 2008, *Phys. Rev. C*, 77, 61304
- Tsang M. B. et al., 2012, *Phys. Rev. C*, 86, 15803
- Van Schelt J. et al., 2013, *Phys. Rev. Lett.*, 111, 61102
- Vescovi D., Reifarth R., Cristallo S., Couture A., 2022, *Frontiers Astron. Space Sci.*, 9
- Wang R., Chen L.-W., 2015, *Phys. Rev. C*, 92, 31303
- Wang N., Liu M., Wu X., Meng J., 2014, *Phys. Lett. B*, 734, 215
- Wang M., Huang W. J., Kondev F. G., Audi G., Naimi S., 2021, *Chin. Phys. C*, 45, 30003
- Watson D. et al., 2019, *Nature*, 574, 497
- Weizsäcker C. F., 1935, *Z. Phys.*, 96, 431
- Wilkinson D. H., 1956, *Physica*, 22, 1039
- Wu M.-R., Fernández R., Martínez-Pinedo G., Metzger B. D., 2016, *MNRAS*, 463, 2323
- Yüksel E., 2021, *Nucl. Phys. A*, 1014, 122238

This paper has been typeset from a $\text{\TeX}/\text{\LaTeX}$ file prepared by the author.